Chemical Engineering Journal 500 (2024) 157358

Contents lists available at ScienceDirect

Chemical Engineering Journal

journal homepage: www.elsevier.com/locate/cej

4D printable and recyclable two-way shape memory butadiene rubber as ultrasensitive, longer-lasting, and lower-cost fire warning sensors

Xiaowei Mu, Guoqiang Li *

Department of Mechanical & Industrial Engineering, Louisiana State University, Baton Rouge, LA 70803, United States

ARTICLE INFO

Keywords:
Butadiene rubber
4D printing
Recyclability
Two-way shape memory effect
Fire warning

ABSTRACT

Fire sensors have been widely used for early warning of fire in confined space in buildings. However, the currently used fire sensors cannot achieve high sensitivity, long service life, and low cost at the same time. In this work, 4D printable and recyclable two-way shape memory polymers (2 W-SMPs), which are made of a butadiene rubber (P-80), have been designed for fire warning sensor with ultra-high sensitivity, longer-lasting service life, and lower-cost. The P-80 displays a high reversible actuation with a crystallization-induced elongation (CIE) and a melting-induced contraction (MIC) as large as 99.3 % and 90.4 %, respectively. The designed fire sensor exhibits an average respond time as fast as 0.2 s and can be reused for more than 20 times. The mechanism for the excellent two-way shape memory effect and recyclability of the P-80 has been revealed. The entropy and enthalpy increase is the primary reasons for the large MIC in P-80, which contributes to 76.1 % and 23.9 % of MIC, respectively. The recyclability of the P-80 is caused by the reconstruction of C = C bond via olefin metathesis reaction, resulting in the dynamic topology reformation. This work provides a guideline for development of 4D printable and recyclable 2 W-SMPs.

1. Introduction

Fire in confined spaces in buildings poses significant hazards to both life and property [1,2]. Fire sensor, as an important strategy for early warning of building fire, has been widely used. Currently, various fire sensors such as heat sensor, gas sensor, smoke sensor, and flame sensor have been commercialized [3]. Most of the commercialized fire sensors show a long response time (> 100 s) but long service lifespan [4], except for flame sensor (< 5 s) [5]. However, flame sensor is of high cost. Apart from the commercialized fire sensors, diverse novel fire sensors with high sensitivity based on different mechanisms including resistance change [6–11], color transition [12,13], and thermal-resistance change [14–16] have also been reported. The reported minimal fire alarm response time (graphene oxide-based fire sensor) is around 0.25 s [17]. However, most of those new fire sensors exhibit some limitations such as short service life (can only be used once), high cost, nonrecyclable material, and uncustomed structure design. Therefore, it is crucial to develop new fire sensors with more comprehensive performance.

Two-way shape memory polymers (2 W-SMPs) are a type of smart materials that expand upon cooling and contract upon heating. Their shape transition in response to external temperature change is reversible and repeatable [18,19]. It has been reported that most of polymers with two-way shape memory effect (2 W-SME) are semi-crystalline elastomeric polymer networks [20]. Most of 2 W-SMPs exhibit reversible crystallization-induced elongation (CIE) upon cooling and melting-induced contraction (MIC) upon heating [21,22]. Except for crystallization/melting transition, our group also proposed that entropy change is also a reason why semi-crystalline elastomeric polymer networks exhibit two-way shape memory effect in the rubbery state [23,24]. A large number of 2 W-SMPs have been developed based on the above mechanism including liquid crystalline elastomers, poly(octylene adipate), poly(Ɛ-caprolactone), oligo(pentadecalactone), ionomer, polyurethane, poly(ethylene-co-vinyl acetate), and poly(1,4-butadiene) (PBD) [25–33]. It is reported that the PBD displays the highest reversible actuation in response to the temperature change among all reported 2 W-SMPs [19]. Thus, if PBD is designed as a fire warning system (FWS), it will show great potential in improving temperature sensitivity and cycle lifespan of the FWS considering its large actuation strain and reversible shape transition.

The olefin metathesis reaction, also known as a model of "green chemistry", refers to the process of breaking and recombination of C = C bonds under the action of a metal catalyst. The C = C bonds in the cross-

* Corresponding author.
E-mail address: lguoqi1@lsu.edu (G. Li).

https://doi.org/10.1016/j.cej.2024.157358
Received 30 August 2024; Received in revised form 7 October 2024; Accepted 1 November 2024
Available online 2 November 2024

linked polymer networks are rapidly exchanged via olefin metathesis reaction, resulting in the topology of the cross-linked network being dynamically altered [34–36]. It displays great potential for designing environmental-friendly recyclable cross-linked polymers. A malleable but insoluble cross-linked PBD has been designed based on olefin metathesis [37]. The key to achieving the recyclable cross-linked PBD is the Grubbs 2nd generation catalyst. It is not only stable in air, but can also maintain high catalytic activity even in the presence of water, alcohol or acid [38].

Digital light processing (DLP) 3D printing, as an emerging manufacturing method, allows to produce complex geometries with high precision that may be difficult or impossible to achieve with traditional manufacturing methods [39–41]. If the PBD can be 3D printed through DLP, it is expected that a 4D printable FWS with a customized structure can be designed to alarm fire in complex and confined spaces. However, the viscosity of commercialized PBD is too high to do 4D printing due to its high molecular weight. Although low molecular weight *cis*-1,4-butadiene shows low viscosity, it is difficult to synthesize a PBD with good mechanical performance based on 4D printing techniques due to its low degree of polymerization.

The objective of this work is to integrate large reversible actuation, 3D or 4D printability, and recyclability into one polymer network as fire sensors. To achieve the objective, this work intends to adopt a blend of low molecular weight *cis*-1,4-butadiene (polyvest 110) and high molecular weight *cis*-PBD to prepare 4D printable and recyclable two-way shape-memory-PBD based FWS in terms of click chemistry and olefin metathesis reaction. A 4D printable cross-linked PBD with desirable mechanical performance can be synthesized due to the high activity of click reaction and low viscosity of low molecular weight *cis*-1,4-butadiene. An environmental-friendly and recyclable FWS with ultra-high sensitivity, long service lifespan, and customized structure design can be realized owing to the large reversible actuation of PBD, recombination of C = C bond through olefin metathesis reaction, and 3D printing technology.

2. Results and discussion

2.1. Preparation and characterization of crosslinked poly(1,4-butadiene)

Conventional PBD with high molecular weight is impossible to do DLP 4D printing due to its high viscosity. However, as shown in Fig. 1 a and b, the crosslinked poly(1,4-butadiene) (P-80) composed of low molecular weight polyvest 110, high molecular weight *cis* PBD and crosslinking agent trimethylolpropane tris(3-mercaptopropionate) (TPMP) is prepared through an DLP 3D printer due to the diluting effect of low-viscosity polyvest 110. In addition to P-80, we also have two more categories of samples, P-80–5 and P-80–15. When P-80 was immersed into Grubbs 2nd generation catalyst solution for 5 min, it is named as P-80–5; when P-80 was immersed into Grubbs 2nd generation catalyst solution for 15 min, it is named as P-80–15. The detailed synthesis route for P-80 has been shown in Fig. 1 c. The P-80 is synthesized based on the Thiol-Ene "click reaction" between TPMP and PBD or polyvest 110. In Fig. 1e, the peaks centered at 2569 and 1743 cm^{-1} are −SH and C = O bond from the TPMP [42,43]. The peaks located at 1259 and 1238 cm^{-1} are asymmetric stretch vibration of C-O-C bond. The peak at 1153 cm^{-1} is symmetrical stretching vibration of C-O-C bond [44–46]. The disappearance of −SH and appearance of C-S bond (698 cm^{-1}) and C-O-C bond on P-80 proves that the P-80 has been prepared successfully [43]. The thermal stability of P-80 decreases compared with that of uncross-linked PBD and polyvest 110 (Figure S1), which is caused by the low thermal stability of crosslink agent TPMP. The crosslinked P-80 can be recycled through the olefin metathesis reaction. The detailed process is shown in Fig. 1 d. The key to achieve the recyclability of P-80 is C = C bond recombination. Thus, a certain amount of C = C bonds

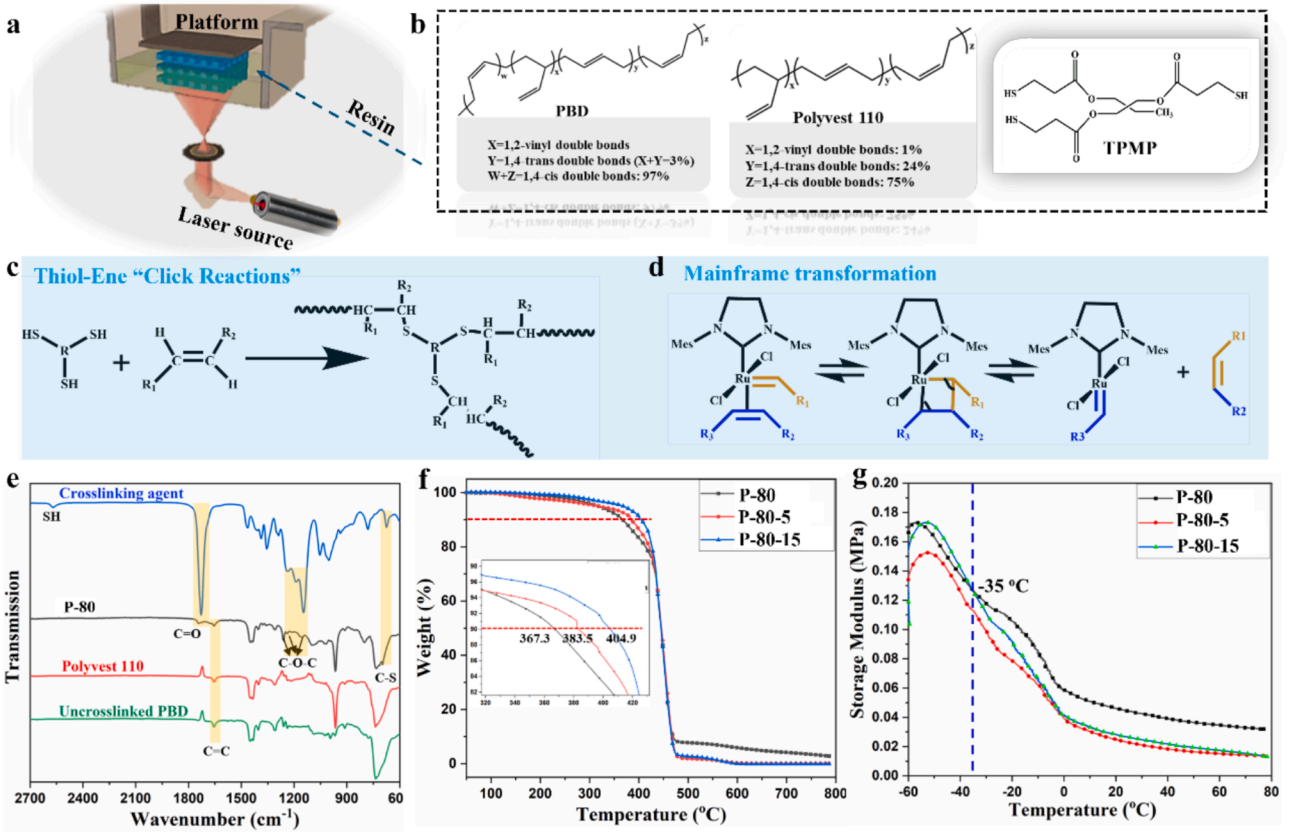

Fig. 1. Preparation and characterization of PBD. a) Schematic illustration of DLP 3D printing. b) Chemical structure of raw materials. c) Synthesis of P-80 based on Thiol-Ene "click reaction". d) The mechanism of olefin metathesis reaction. e) The FTIR curves, f) TGA curves under nitrogen, and g) storage modulus of samples.

(Fig. 1e) are reserved in the crosslinked P-80 and a Grubbs 2nd generation catalyst with a high catalytic activity is adopted. The thermal and mechanical properties of P-80 have been regulated by the olefin metathesis reaction without changing its topology structure. The FTIR curves of P-80 and Grubbs 2nd generation catalyst modified P-80 are the same (Fig. S2). However, the crystallization temperature (T_m) of P-80 decreases from −13 to −27.5 °C with increased content of Grubbs 2nd generation catalyst (Fig. S3). The temperature at 10 % weight loss ($T_{10\ wt\%}$) of P-80 under nitrogen environment increases from 367.3 °C to 404.9 °C with the increase in the content of Grubbs 2nd generation catalyst. The Grubbs 2nd generation catalyst may work as the stabilizers, which can increase the resistance to thermal degradation. However, the char residue at 700 °C of P-80 decreases from 4.2 wt% to 0.1 wt% with the increase in the content of Grubbs 2nd generation catalyst (Fig. 1f and Fig. S4). The sample's molecular structure become more homogeneous due to reconstruction of network topology caused by olefin metathesis reaction. The polymer with a more homogeneous topology may degrade more uniformly, reducing the likelihood of leaving behind solid char residues. The storage modulus of P-80 which was immersed into Grubbs 2nd generation catalyst solution for 15 min (P-80–15) is larger than that of untreated one below −35 °C. However, the storage modulus of P-80–15 above −35 °C is smaller than that of P-80 (Fig. 1g). Besides, the loss modulus of P-80–15 is larger than that of P-80 (Fig. S5). It proves that the viscoelasticity of P-80 has been enhanced after olefin metathesis reaction.

2.2. Recyclability of P-80

The P-80 was immersed into $CHCl_3$ with stirring to test its recyclability. The crosslinked P-80 can be dissolved into $CHCl_3$ completely or even be melted at 80 °C due to the olefin metathesis reaction (Fig. 2 a and Fig. S6). The Grubb 2nd generation catalyst shows high stability. Its chemical structure is the same even after UV-curing (Figure S 7). After evaporating the $CHCl_3$ and UV curing, a cubic P-80 sample can be reshaped into round piece, love heart or hexagonal star (Fig. 2a and Fig. S6). However, P-80 without Grubb 2nd generation catalyst cannot be dissolved by $CHCl_3$ even after 2 days of immersion (Fig. S8). The mechanical performance of the recycled P-80 has been displayed in Fig. 2b and Fig. S9. The breaking strength increases but elongation at break decreases with the increased number of cycles. The breaking strength and elongation at break of P-80 are 16.5 KPa and 489 %, respectively. The breaking strength of P-80 after three recycling cycles (P-80^{3}rd) is increased by 73 % (28.5 KPa). However, the elongation at break of P-80^{3}rd decreased to 180 % compared with that of original P-80. The reason for the enhanced breaking strength but decreased deformability of P-80^{3}rd persists in the increased crosslinking density. The crosslinking density of P-80^{3}rd increases from 1.854×10^{-5} to 1.68×10^{-4} mol/cm^3 (Fig. 2c). The reason for the increased crosslink density is that we added the photoinitiator again before recycling the samples. The amount of the photoinitiator added was 9 wt% for each recycling cycle. The UV curing condition for each recycling process was the same. Because some new crosslinks may have been formed due to the newly added photoinitiator during each recycling cycle, the crosslinking

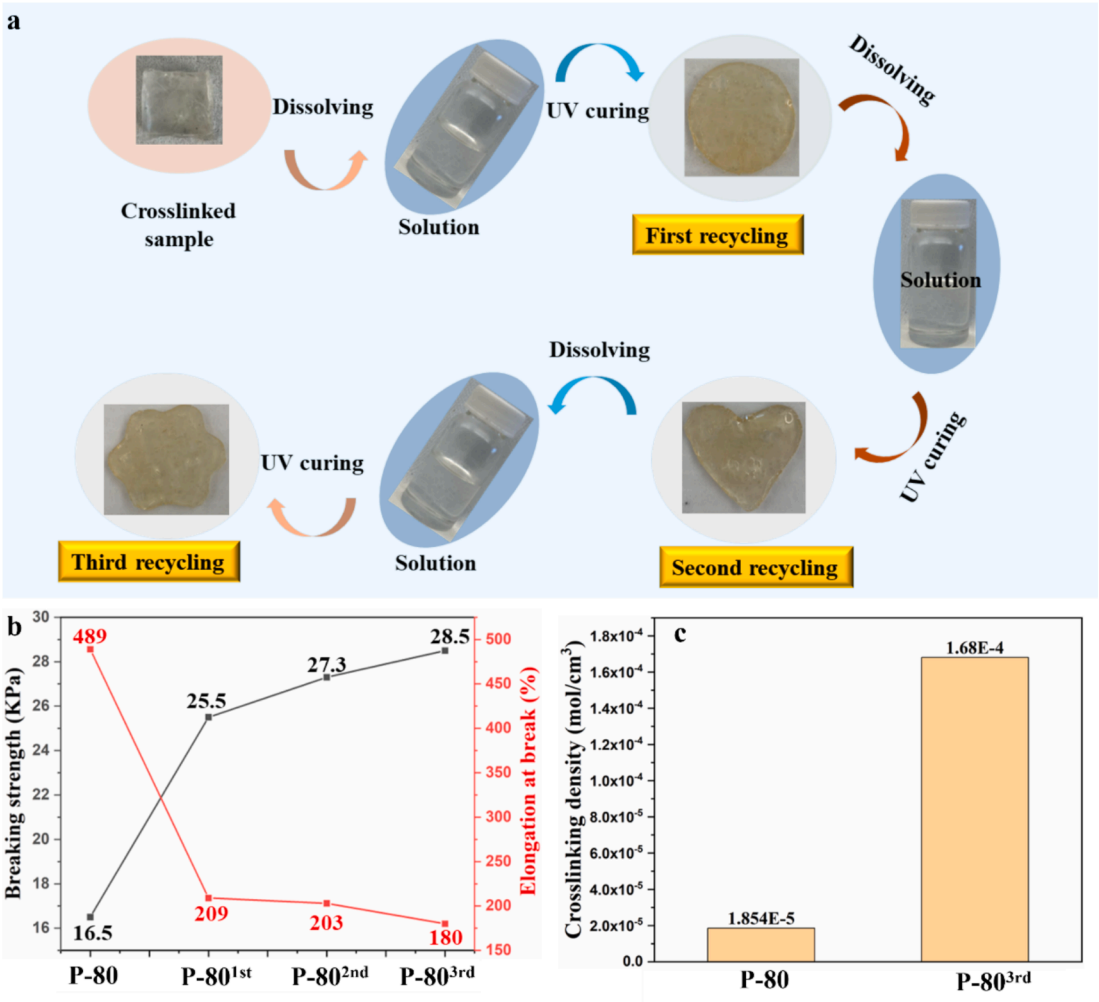

Fig. 2. Recyclability of P-80. a) Recycling process of P-80. b) The mechanical property of P-80 before and after the recycle. c) The crosslinking density of the sample.

density of the recycled sample increased gradually with the increase in the number of the recycling cycles. As a result, the breaking strength of the recycled samples increases but the strain at break decreases as the number of the recycling cycles increases.

2.3. In-depth interpretation of the recyclability of P-80

To better understand why the P-80 can be recycled like a vitrimer, more detailed investigation has been conducted in Fig. 3. As shown in Fig. 3 a, the C = C bond in the cross-linked P-80 can be exchanged via olefin metathesis reaction, resulting in the topology of P-80 being transformed dynamically. Thus, the P-80 with a crosslinked network topology demonstrates the reprocessing-recyclable nature of thermoplastic polymers. During the tensile test, the stiffness of P-80 decreases after adding Grubb 2nd generation catalyst (Fig. 3b), as evidenced by the reduction in the initial slope of the stress–strain curves. This is because the more the content of the Grubb 2nd generation catalyst, the more the C = C bonds in P-80 that can be broken and recombined. The elongation at break of P-80–15 increases by 68 % compared with that of P-80. The tensile strength of P-80 decreases first then increases with increased content of Grubb 2nd generation catalyst. The tensile strength of P-80–15 is lower than that of P-80 but higher than that of P-80 which was immersed into Grubbs 2nd generation catalyst solution for 5 min (P-80–5). The P-80–15 with high content of Grubb 2nd generation catalyst shows a higher C = C bond reconstruction rate, which may display a better self-healing properties, resulting in enhancement in tensile strength. The stress relaxation and creep tests have also been conducted to investigate the effects of olefin metathesis reaction on the recyclability of P-80. The stress attenuation and stiffness reduction during stress relaxation are shown in Fig. 3 c and Fig. S10. The normalized stress and stiffness at 30 min of treated P-80 are lower than that of untreated one. However, the normalized stress and stiffness at 30 min of P-80–15 are larger than that of P-80–5. This is consistent with tensile strength results shown in Fig. 3b. The creep performances of the samples are shown in Fig. 3d-g and Fig. S11. There are two stages in creep test. The first stage is the creep stage from 0 to 10 min. The second stage is the recovery stage from 10 to 30 min. In the first stage, the strain and creep compliance of Grubb 2nd generation catalyst treated P-80 are significantly larger than that of untreated original P-80 (Fig. 3 d, f and Fig. S11). The maximum strain of P-80–15, P-80–5, and P-80 are 62.28 %, 39.34 % and 12.06 %, respectively (Fig. 3e). This is in line with the elongation at break results shown in Fig. 3b. In the second stage, the recovery compliance of the treated P-80 is larger than that of the pure P-80 (Fig. 3g). The remaining strain during the recovery stage at 20 min of P-80–15 is even smaller than that of P-80–5 (Fig. 3d and e). Polymers are viscoelastic materials [47–49]. The restriction of network topology on the movement of P-80 polymer chains and segments has been weakened by the olefin metathesis reaction, resulting in the enhancement in

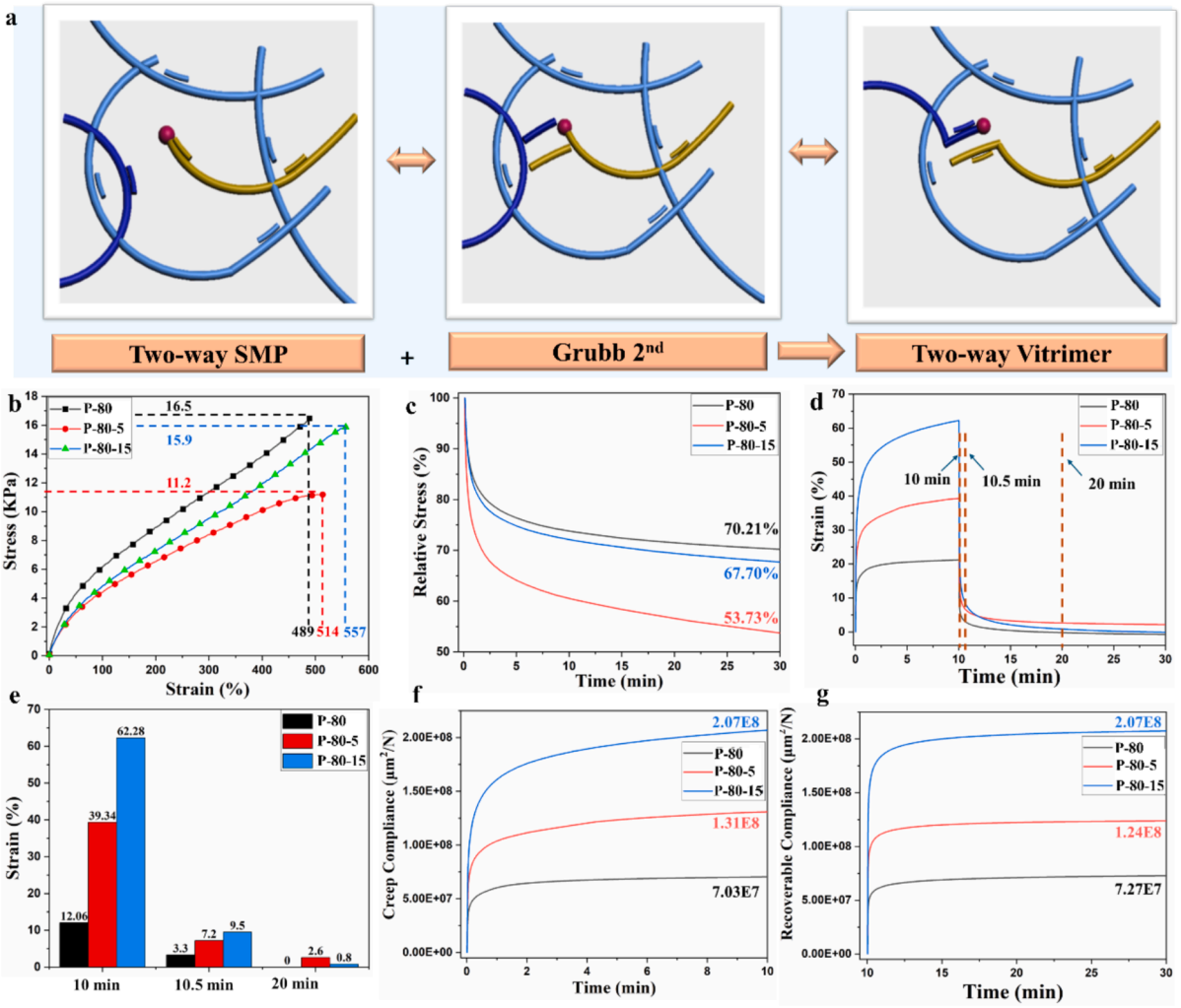

Fig. 3. In-depth interpretation of the recyclability of P-80. a) Schematic illustration of rearrangement of network topology of P-80 based on olefin metathesis reaction. b) Tensile stress–strain curves of samples. c) Normalized stress-time curves of samples. d) Strain-time curves of samples. e) Strain of samples at different time after the creep. f) Creep compliance, and g) recoverable compliance of samples.

mobility of P-80. Thus, the creep and recovery compliance of treated P-80 are increased. In other words, the above results further prove that the olefin metathesis reaction does cause the reconstruction of the P-80 network topology. The fundamental reason why the P-80 has recyclability is the breaking and recombining of C = C bonds within the P-80 network.

2.4. Two-way shape memory performance of P-80

As shown in Fig. 4 a, P-80 displays a typical two-way shape memory performance with a repeatable crystallization-induced elongation (CIE) and melting-induced contraction (MIC) in response to temperature change. The CIE and MIC increase with increase in the external force (from 0.004 MPa to 0.009 MPa). The P-80 displays a high degree of repeatable and reversible actuation in the loading direction between −40 to 60 °C compared with the reported works (Fig. 4e). The CIE and MIC of P-80 with a constant force of 0.009 MPa are as high as 99.3 % and 90.4 %, respectively (Fig. 4b). The stress evolution of 300 % stretched P-80 with temperature is shown in Fig. 4c to further prove its two-way shape memory performances. The stress of 300 % stretched P-80 decreases during cooling but increases during heating. This trend is contrary to polymer without two-way shape memory performances. For P-80, it expands during cooling and contracts during heating. To maintain a stable 300 % strain, the stress of P-80 decreases during colling but increases during heating. The thermal conductivity of the stretched P-80 is displayed in Fig. 4d and Fig. S12. The P-80 with two-way shape memory performance (under 300 % tensile strain) exhibits a higher thermal conductivity and thermal effusivity compared with that of P-80 without two-way shape memory performance. The reason that the thermal conductivity is higher along the loading direction can be explained as follows. The orientation of polymer chains plays a crucial role in determining the thermal conductivity of polymers due to the way that heat is transferred through the molecular structure. Thermal conductivity is the ability of a material to transfer heat, and in polymers, this process largely depends on the movement of phonons (lattice vibrations) or the vibrational energy transfer through the polymer chains. The P-80 was stretched to 300 % in Fig. 4d. The polymer chain of P-80 with 300 % strain is well-oriented. Thus, there is less scattering of phonons because the aligned chains created a more direct pathway for heat transfer. As a result, heat conduction is more efficient along the direction of chain alignment [50].

2.5. The mechanisms for the good two-way shape memory performance of P-80

The crystallization/melting transition of P-80 has been tested to further understand why P-80 shows a large CIE and MIC. The P-80 shows a T_m of −13 °C (Fig. 5a). Besides, the stretched P-80 transferred from transparent to partly opaque after being cooled by liquid nitrogen (Fig. S13 and Video 1), suggesting transition from amorphous to crystalline morphology. The T_m of P-80 is within the two-way shape memory test temperature range (−40–60 °C). Thus, the crystallization/melting transition is indeed one of the reasons that why P-80 expands upon cooling and contracts upon heating. However, the strain changes of P-80 from −40 to −13 °C is only 23.7 %. It is much smaller than strain changes (75.6 %) from −13 to 60 °C (Fig. 5b). It proves that the crystallization/melting transition of P-80 is not the main reason that causes the large CIE and MIC of P-80. We try to figure it out according to thermodynamics. The enthalpy and entropy of P-80 will change with temperature [51,52]. The crystallization/melting transition is the typical enthalpy change. Changes in bond lengths and bond angles will cause enthalpy changes, and chain segment motion and polymer chain orientation will cause entropy change [53]. As shown in Fig. 5c, we divided stress and stress change rate of P-80 into two stages based on the temperature. The first stage including the crystallization/melting transition is named as enthalpy change stage. Due to the low temperature, the chain segment motion is restricted by the crystallization zone of the polymer. Only the bond lengths and bond angles can be changed. Thus, the enthalpy change is dominant. The second stage in Fig. 5c is named as entropy change stage. The changes in chain segment motion and polymer chain orientation will occur. In Fig. 5c, the stress change rate at −40 °C is around 0, which proves that the stretched chain has been

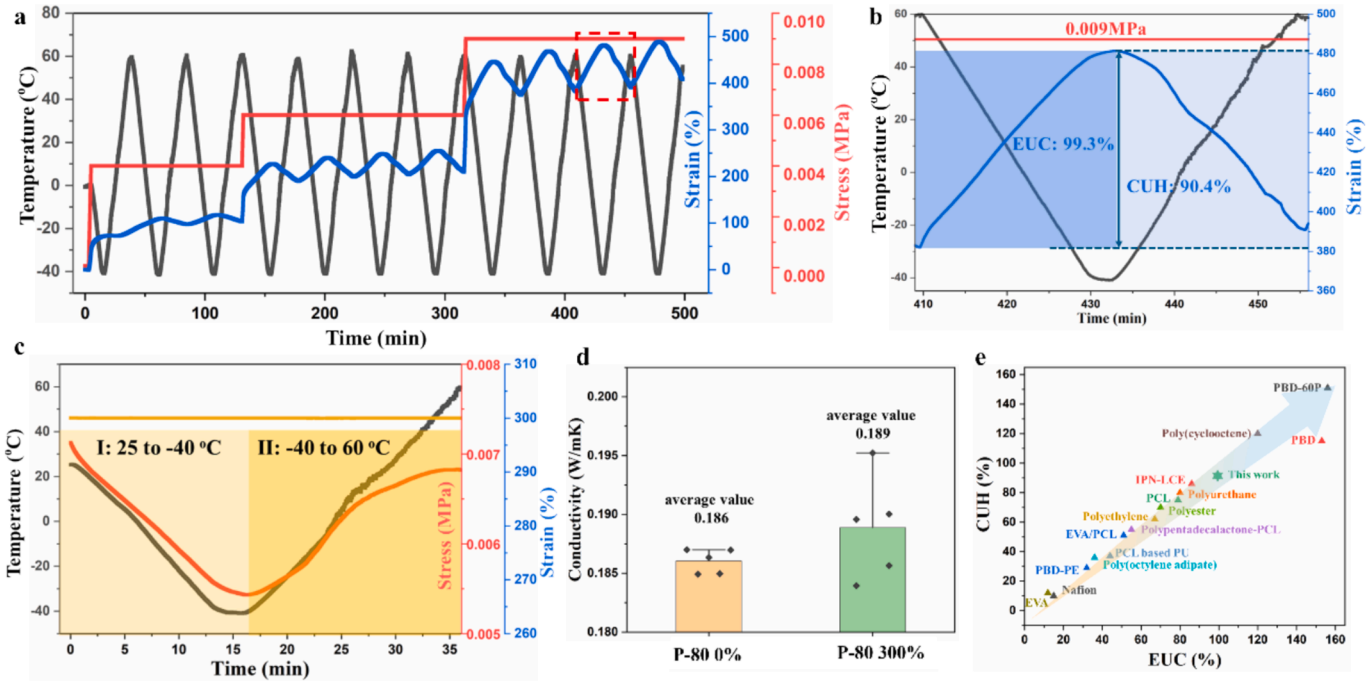

Fig. 4. Two-way shape memory effect. a) Temperature-strain–time curves of P-80 under different external force. b) Temperature-strain–time curves of P-80 at an external force of 0.009 MPa. c) Temperature-stress-time curves of P-80 at a constant strain of 300 %. d) The thermal conductivity of P-80 at 0 % and 300 % strain. e) The reported MIC and CIE [19,23,25,27–29,59–67].

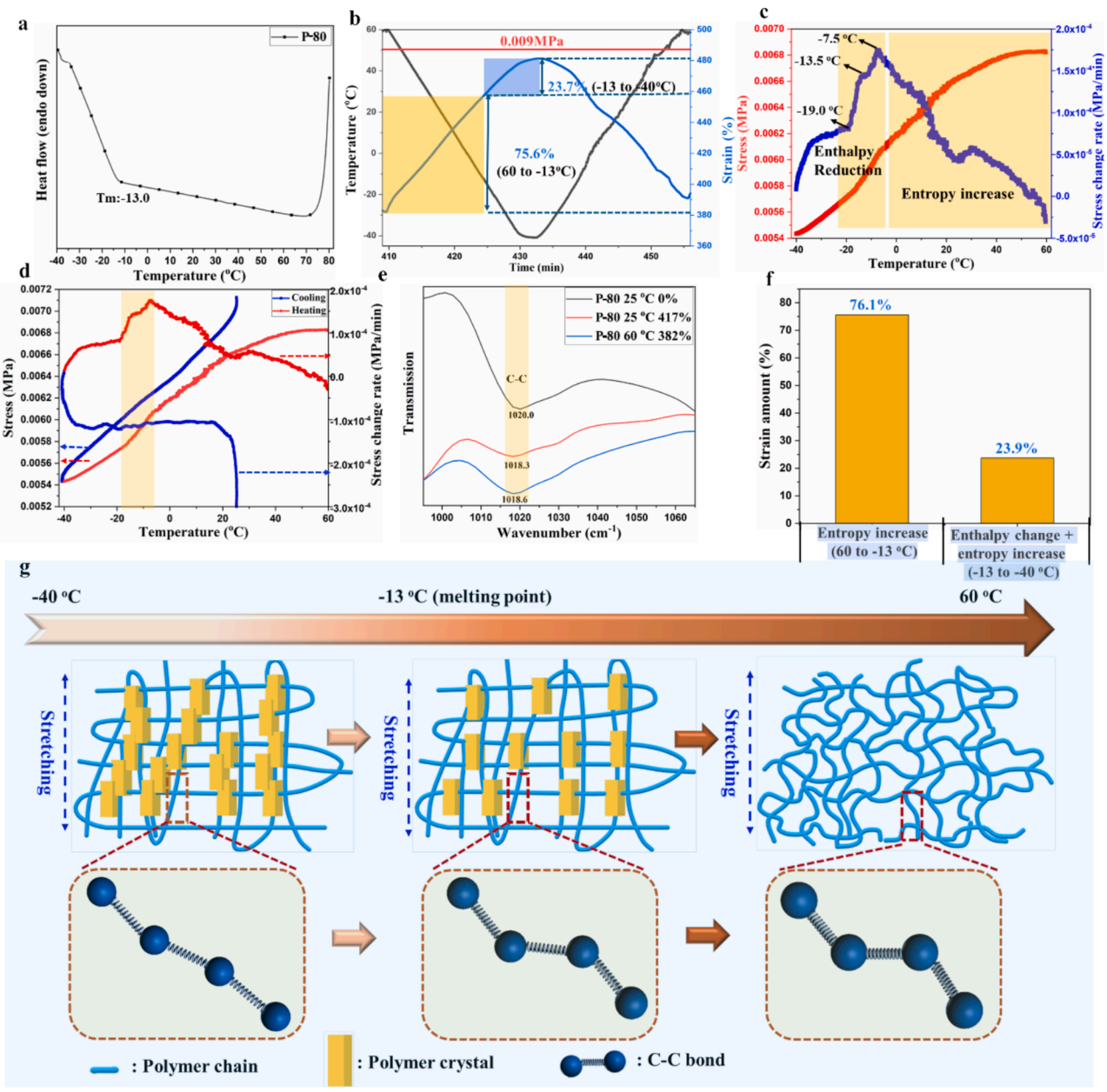

Fig. 5. The reasons for good two-way shape memory performance of P-80. a) DSC curves of the sample. b) Temperature-strain–time curve of P-80. c, d) Stress-stress change rate-temperature curves of P-80 with a constant strain of 300 %. e) FTIR curves of the sample. f) The amount of strain of P-80 based on different mechanisms. g) Schematic illustration of melting-induced contraction mechanism of P-80.

crystallized [54,55]. The low stress change rate may mainly be caused by changes in bond lengths and bond angles. The stress change rate increases sharply during enthalpy change stage due to the crystallization/melting transition. The three peaks at −19.0, −13.5 and −7.5 °C correspond to crystallization/melting transition zone of P-80, which is within the range detected by DSC. The stress change rate of P-80 starts to decrease with the increase in temperature in the entropy change stage, as shown in Fig. 5c. The stretched polymer chains are oriented. As the temperature increases, the heat absorbed continues to increase, and the oriented polymer chains begin to become disordered (entropy increases). This process corresponds to three steps. First, the stretched bond length is reduced, then the chain segment orientation is restored, and finally, the polymer chain orientation is partially restored. Thus, the stress change rate of P-80 decreases but stress increases with the increase in temperature in the entropy change stage. The stress and stress change rate during the cooling and heating process are shown in Fig. 5d and Fig. S14. The stress change rate peaks (marked area) during the cooling are consistent with that during the heating process, which further proves the occurrence of crystallization/melting transition of P-80. The FTIR curves of P-80 at 25 and 60 °C in Fig. 5b have been displayed in Fig. 5e and Fig. S15. The C-C bond of the unstretched P-80 is at 1020.0 cm^{-1}. During the two-way performance test, the C-C bond (1018.3 cm^{-1}) of P-80 is blue-shifted at 25 °C compared with that of unstretched P-80. This is caused by the increased C-C bond length [56]. When increasing the temperature from 25 to 60 °C, the C-C bond is red-shifted. The P-80 contracts during heating, leading to decrease in C-C bond length. The reasons why P-80 has a large MIC have been shown in Fig. 5f. The entropy increase is the main reason for large MIC of P-80, which contributes to 76.1 % of contraction. The enthalpy increase is only the secondary reason, which provides 23.9 % of contraction. The detailed MIC mechanism of P-80 is sketched in Fig. 5g. During the heating process, the crystallinity of semi-crystalline P-80 decreases, the C-C bond

length of P-80 decreases, and the bond angle changes due to the enthalpy and entropy increase from −40 to −13 °C. When the temperature reaches 60 °C, which is well above the crystallization/melting transition temperature, the P-80 becomes amorphous. The stretched C-C bond, the oriented chain segment, and the polymer chain of P-80 have been gradually relaxed, leading to entropy increase.

2.6. The application of 4D printable P-80

A series of P-80 s in different shapes including rectangles, circles, flowers, and butterflies are 4D printed as shown in Fig. 6. A fire warning system (FWS) based on 4D printed P-80 has been designed (Fig. 6d). When the flame warms up P-80 stripe, the P-80 stripe shrinks rapidly. The P-80 stripe brings the metal wire up, and the circuit is connected. As a result, the alarm light is lighted up. When the flame is removed, the P-80 stripe is cooled and returns to its original length quickly, causing the circuit to open and the alarm light to go out. The digital images and video of the FWS have been shown in Fig. 6a-c and Video S2. The FWS exhibits the ultra-high fire sensitive and long-lasting fire warning cycles compared with reported works (Fig. 6g). The average respond time and average duration of the FWS are 0.2 s and 1.7 s, respectively. (Fig. 6e and Fig. S16). The reusing cycles of the FWS are more than 20 times (Fig. 6f). The reported FWS not only combines advantages of high fire alarm sensitivity but also the long-lasting cycling use (Fig. 6g). Most reported FWSs can only be used for once although its sensitivity is even as high as 0.25 s [17]. The working mechanism of the recycled FWS reported is based on energy band theory of semiconductor [57]. When the flame contacts the semiconductor, the electrons in the valence band will gain energy and jump to the conduction band, resulting in a significant increase in electrical conductivity [58]. However, the conductivity of semiconductor materials is low before contacting the flame, which will inevitably sacrifice the alarm sensitivity of the FWS. The working mechanism of FWS in this work is based on reversible CIE and MIC of 2 W-SMPs. P-80 displays a high reversible deformation ratio and a large deformation rate in response to the temperature change (Fig. 5), which overcomes the disadvantages of the reported FWSs, giving the FWS designed in this work ultra-high fire sensitivity and long cycle lifespan. Besides, P-80 is environmental-friendly and recyclable, 4D printable, and inexpensive. Therefore, P-80 based FWS has a great application potential.

In addition to being used for fire warning, 4D printed P-80 can also be used for information storage. The logo of Louisiana State University (LSU) can be printed on the surface of P-80 (Fig. 6j). When a high intensity flashlight shines on the P-80, the letters of "LSU" appear. When the high intensity flashlight is removed, the "LSU" disappears (Fig. 6k and Video 3). The letters of "LSU" are first embossed on the 4D printed P-

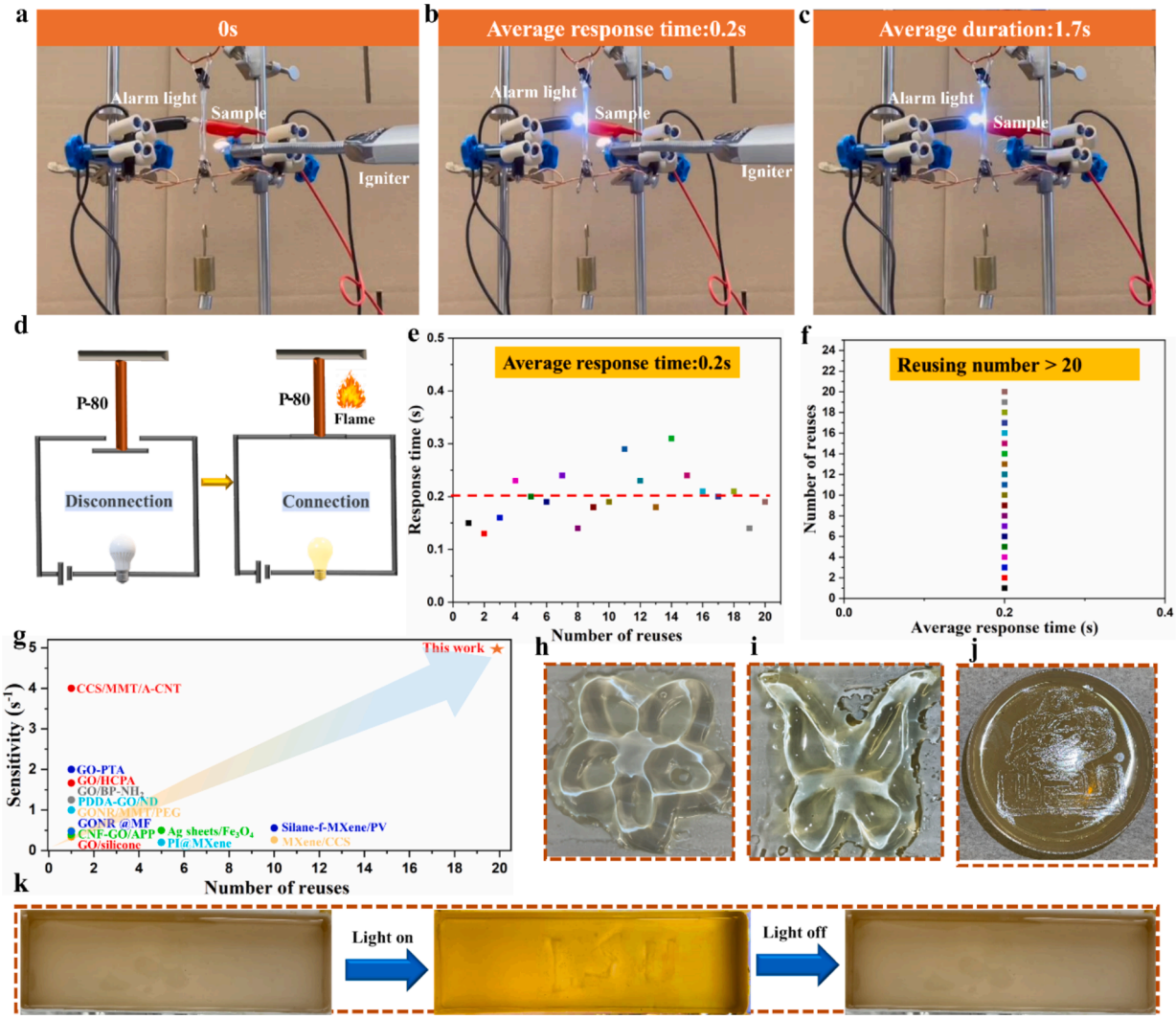

Fig. 6. Application of 3D printed P-80. a-c) Digital images of 3D printed P-80 based FWS. d) Schematic illustration of working mechanism of FWS. e) Fire alarm sensitivity of FSW. f) Recycle lifespan of FWS. g) Reported fire alarm sensitivity and recycled lifespan [8,17,68–78] 3D printed h) flower, i) butterfly, and j) LSU logo. k) Digital image of stress induced pattern.

80 surface. After the letters of "LSU" are removed, further UV curing is performed. The anisotropy caused by "LSU" is stored inside the P-80 after UV-curing. The anisotropy leads to change in refraction index. Refraction occurs when light passes through the interface of two phases with different refractive indices, resulting in reappearance of the three letters "LSU" when a beam of light shines on the sample. Thus, the "LSU" appears inside the P-80 thin film when light strikes on it.

3. Conclusions

In this work, a 4D printable and recyclable two-way shape memory butadiene rubber (P-80) has been designed as ultra-highly sensitive, longer-lasting, and lower-cost fire warning sensor. The P-80 based 4D printable fire sensor exhibits the ultra-high fire sensitivity (average respond time of 0.2 s) and longer-lasting fire warning cycles (can be reused more than 20 times) compared with reported works due to the high reversible actuation and fast deformation rate in response to temperature change. In addition to being used for fire warning, 4D printed P-80 can also be used for information storage. The letters of "LSU" will appear inside the P-80 thin film after being shined by light due to the storage of anisotropy. The P-80 displays a good two-way shape memory effect with a crystallization-induced elongation (CIE) and a melting-induced contraction (MIC) as large as 99.3 % and 90.4 %, respectively. The mechanism for the good two-way shape memory effect and the in-depth interpretation of the recyclability of P-80 have been revealed. The entropy and enthalpy increase are two main reasons for the large MIC of P-80, which contributes to 76.1 % and 23.9 % of CUH, respectively. During the heating process, the crystallinity of the semi-crystalline P-80 decreases, the C-C bond length of P-80 network decreases, and the bond angle changes due to the enthalpy and entropy increase. The stretched C-C bond, the oriented chain segment and the alignment of the polymer chain in P-80 have been released gradually due to the entropy and enthalpy increase. The recyclability of P-80 is caused by the rapid breaking and recombining of C = C bond within the cross-linked network via olefin metathesis reaction, resulting in the topology being dynamically altered. The breaking strength increases but elongation at break decreases with the increase in the number of recycles. The breaking strength and elongation at break of the P-80 are 16.5 KPa and 489 %, respectively. The breaking strength of P-80 after three recycles (P-80^{3}rd) increases by 73 % (28.5 KPa). The elongation at break of P-80^{3}rd decreases to 180 % compared with that of P-80. This work provides a guideline for development of 4D printable and recyclable two-way shape memory polymer as fire warming sensors, information storage devices, and other high-tech applications.

4. Material and methods

4.1. Preparation of poly(1,4-butadiene)

10 g PBD was first immersed into 190 g $CHCl_3$ for 3 d and then dissolved through mechanical stirring at room temperature for 1 d to prepare PBD solution. Then 80 g PBD solution, 1 g Polyvest 110, 0.15 g 2-hydroxy-2-methylpropiophenone and 0.05 g tris(3-mercaptopropionate) were mixed and dried at room temperature for 2 d. Finally, the mixture was cured in a UV chamber (IntelliRay 600, Uvitron International, USA) for 90 s under 35 % irradiation intensity (232 nm).

4.2. 4D printing of poly(1,4-butadiene)

A mixture containing 77.6 g Polyvest 110, 2.4 g PBD, 0.8 g trimethylolpropane tris(3-mercaptopropionate), 4 g 2-hydroxy-2-methylpropiophenone, and 4 g (Phenylphosphoryl)bis(mesitylmethanone) was added into a digital light processing (DLP) 3D printer (Anycubic Photon Mono X 6 K) with a layer thickness of 0.05 mm, a normal exposure time of 45 s, a bottom exposure time of 60 s, and a bottom layer of 10. The printing accuracy is 5,760 × 3,600 pixels and the horizontal resolution is 34 μm. The power output is 5,500 μw/cm^2, and the maximum printing speed in thickness direction is 80 mm/h.

4.3. Preparation of recyclable poly(1,4-butadiene)

0.02 g Grubbs 2nd generation catalyst was dissolved into 200 mL $CHCl_3$. Then 2 g prepared crosslinked poly(1,4-butadiene) was immersed into above solution for 5 min or 15 min. after that, crosslinked poly(1,4-butadiene) contained Grubbs 2nd generation catalyst were dried at room temperature for 4 h under a vacuum oven. Then crosslinked poly(1,4-butadiene) contained Grubbs 2nd generation catalyst was redissolved into $CHCl_3$ solution containing 3 wt% 2-hydroxy-2-methylpropiophenone and 1 wt% trimethylolpropane tris(3-mercaptopropionate) at room temperature under stirring for 1 d. The reprepared poly(1,4-butadiene) was dried out under a vacuum oven and then cured in a UV chamber for 40 s under 35 % irradiation intensity (232 nm). Repeating the above steps for three times.

4.4. Preparation of fire warning system

The general idea was as follows: the power supply, LED light and wires formed a series circuit. The P-80 was designed as a switch. When the temperature rose, the switch was turned on and the LED light turned on. When the temperature dropped, the switch was turned off and the LED light turned off. The specific design of the switch was as follows: a P-80 (5 × 1 × 0.3 cm^3) was hung vertically, and a weight of 125 g and a horizontally placed copper wire were hung below the P-80. The series circuit consisting of the power supply, LED light and wires was specifically designed as follows: one end of the black wire was connected to the LED light and the other end was fixed on the clip. One end of the red wire was connected to the LED light and the other end was also fixed to another clip. The heights of the two wires fixed by the clips were the same. The copper wire placed horizontally was 1 cm below the electrical wire.

CRediT authorship contribution statement

Xiaowei Mu: Writing – original draft, Visualization, Validation, Methodology, Investigation, Formal analysis, Data curation, Conceptualization. **Guoqiang Li:** Writing – review & editing, Supervision, Resources, Project administration, Funding acquisition, Conceptualization.

Declaration of competing interest

The authors declare that they have no known competing financial interests or personal relationships that could have appeared to influence the work reported in this paper.

Acknowledgements

This work is funded by the US National Science Foundation under Grant Number OIA-1946231 and the Louisiana Board of Regents for the Louisiana Materials Design Alliance (LAMDA), the US National Science Foundation under grant number HRD-1736136.

Appendix A. Supplementary data

Supplementary data to this article can be found online at https://doi.org/10.1016/j.cej.2024.157358.

Data availability

Data will be made available on request.

References

[1] D. Cortés, D. Gil, J. Azorín, F. Vandecasteele, S. Verstockt, A review of modelling and simulation methods for flashover prediction in confined space fires, J. Appl. Sci. 10 (16) (2020) 5609.

[2] X. Mu, Z. Jin, F. Chu, W. Cai, Y. Zhu, B. Yu, L. Song, Y. Hu, High-performance flame-retardant polycarbonate composites: Mechanisms investigation and fire-safety evaluation systems establishment, Compos. Part B-Eng. 238 (2022) 109873.

[3] A. Gaur, A. Singh, A. Kumar, K.S. Kulkarni, S. Lala, K. Kapoor, V. Srivastava, A. Kumar, S.C. Mukhopadhyay, Fire sensing technologies: A review, EEE Sens. J. 19 (9) (2019) 3191–3202.

[4] X. Li, A. Vázquez-López, J. Sánchez del Río Sáez, D.-Y. Wang, Recent advances on early-stage fire-warning systems: mechanism, performance, and perspective, Nano-Micro Lett. 14 (1) (2022) 197.

[5] L. Xu, Y. Yan, A new flame monitor with triple photovoltaic cells, Measurement 55 (4) (2006) 1416–1421.

[6] C.H. Liu, C.C. Chen, Z.W. Guo, Y.K. Fuh, T.T. Li, Self-powered fire alarm system with layer-by-layer graphene oxide/chitosan nanocoating of flame-retardant nanofilms, Adv. Mater. Technol.-US 8 (21) (2023) 2300914.

[7] L. Cao, Q. Liu, J. Ren, W. Chen, Y. Pei, D.L. Kaplan, S. Ling, Electro-blown spun silk/graphene nanoionotronic skin for multifunctional fire protection and alarm, Adv. Mater. 33 (38) (2021) 2102500.

[8] M. Mao, K.-X. Yu, C.-F. Cao, L.-X. Gong, G.-D. Zhang, L. Zhao, P. Song, J.-F. Gao, L.-C. Tang, Facile and green fabrication of flame-retardant $Ti_3C_2T_x$ MXene networks for ultrafast, reusable and weather-resistant fire warning, Chem. Eng. J. 427 (2022) 131615.

[9] Q. Wu, L.-X. Gong, Y. Li, C.-F. Cao, L.-C. Tang, L. Wu, L. Zhao, G.-D. Zhang, S.-N. Li, J. Gao, Efficient flame detection and early warning sensors on combustible materials using hierarchical graphene oxide/silicone coatings, ACS Nano 12 (1) (2018) 416–424.

[10] Y.-B. Shen, K.-X. Yu, Y.-J. Wang, Y.-H. Qu, L.-Q. Pan, C.-F. Cao, K. Cao, J.-F. Gao, Y. Shi, P. Song, Color adjustable, mechanically robust, flame-retardant and weather-resistant TiO_2/MMT/CNF hierarchical nanocomposite coatings toward intelligent fire cyclic warning and protection, Compos. Part B-Eng. 271 (2024) 111159.

[11] Y.-J. Wang, B.-F. Guo, L.-D. Peng, Y. Li, C.-F. Cao, G.-D. Zhang, J.-F. Gao, P. Song, Y.-Q. Shi, K. Cao, Recent progress on MXene-based advanced nanocomposite materials for thermal radiation protection and fire safety, Adv. Nanocompos. 1 (2024) 217–239.

[12] Y.Y. Xu, L.Y. Huang, J. Long, R.Z. Zhang, Z.X. Zhong, L. Yang, L. Liu, Y.D. Huang, Reversible thermochromic POSS-Metal Films for early warning, Compos. Sci. Technol. 217 (2022) 109083.

[13] T. Fu, X. Zhao, L. Chen, W.S. Wu, Q. Zhao, X.L. Wang, D.M. Guo, Y.Z. Wang, Bioinspired Color Changing Molecular Sensor toward Early Fire Detection Based on Transformation of Phthalonitrile to Phthalocyanine, Adv. Funct. Mater. 29 (8) (2019) 1806586.

[14] Q. Jiang, Y. Wan, Y. Qin, X. Qu, M. Zhou, S. Huo, X. Wang, Z. Yu, H. He, Durable and Wearable Self-powered Temperature Sensor Based on Self-healing Thermoelectric Fiber by Coaxial Wet Spinning Strategy for Fire Safety of Firefighting Clothing, Adv. Fiber Mater. (2024) 1–15.

[15] H. He, Y. Qin, Z. Zhu, Q. Jiang, S. Ouyang, Y. Wan, X. Qu, J. Xu, Z. Yu, Temperature-arousing self-powered fire warning E-textile based on p–n segment coaxial aerogel fibers for active fire protection in firefighting clothing, Nano-Micro Lett. 15 (1) (2023) 226.

[16] Z. Ding, C. Du, W. Long, C.-F. Cao, L. Liang, L.-C. Tang, G. Chen, Thermoelectrics and thermocells for fire warning applications, Sci. Bull. 68 (2023) 3261–3277.

[17] J.Y. Chen, H.L. Xie, X.J. Lai, H.Q. Li, J.F. Gao, X.R. Zeng, An ultrasensitive fire-warning chitosan/montmorillonite/carbon nanotube composite aerogel with high fire-resistance, Chem. Eng. J. 399 (2020) 125729.

[18] J.J. Li, W.R. Rodgers, T. Xie, Semi-crystalline two-way shape memory elastomer, Polymer 52 (23) (2011) 5320–5325.

[19] X.M. Feng, G.Q. Li, Photo-crosslinkable and ultrastable poly(1,4-butadiene) based organogel with record-high reversible elongation upon cooling and contraction upon heating, Polymer 262 (2022) 125477.

[20] S. Li, Z. Li, S. Mei, X. Chen, B. Ding, Y. Zhang, W. Zhao, X. Zhang, Z. Cui, P. Fu, 4D Printed Thermoplastic Polyamide Elastomers with Reversible Two-Way Shape Memory Effect, Adv. Mater. Technol.-US 8 (13) (2023) 2202066.

[21] M. Zare, M.P. Prabhakaran, N. Parvin, S. Ramakrishna, Thermally-induced two-way shape memory polymers: Mechanisms, structures, and applications, Chem. Eng. J. 374 (2019) 706–720.

[22] K.J. Wang, Y.G. Jia, C.Z. Zhao, X.X. Zhu, Multiple and two-way reversible shape memory polymers: Design strategies and applications, Prog. Mater. Sci. 105 (2019) 100572.

[23] L. Lu, J.B. Cao, G.Q. Li, Giant reversible elongation upon cooling and contraction upon heating for a crosslinked cis-poly(1,4-butadiene) system at temperatures below zero Celsius, Sci. Rep.-UK 8 (2018) 14233.

[24] C. Yan, Q. Yang, G. Li, A phenomenological constitutive model for semicrystalline two-way shape memory polymers, Int. J. Mech. Sci. 177 (2020) 105552.

[25] Q. Yang, W.J. Zheng, W.P. Zhao, C. Peng, J.T. Ren, Q.Z. Yu, Y.M. Hu, X.Q. Zhang, One-way and two-way shape memory effects of a high-strain cis-1,4-polybutadiene-polyethylene copolymer based dynamic network via self-complementary quadruple hydrogen bonding, Polym. Chem.-UK 10 (24) (2019), 3399–3399.

[26] J.M. Laza, A. Veloso, J.L. Vilas, Tailoring new bisphenol a ethoxylated shape memory polyurethanes, J. Appl. Polym. Sci. 138 (2) (2021) 49660.

[27] M. Behl, K. Kratz, U. Noechel, T. Sauter, A. Lendlein, Temperature-memory polymer actuators, P. Natl. Acad. Sci. USA 110 (31) (2013) 12555–12559.

[28] C.A. Tippets, Q.X. Li, Y.L. Fu, E.U. Donev, J. Zhou, S.A. Turner, A.M.S. Jackson, V. S. Ashby, S.S. Sheiko, R. Lopez, Dynamic Optical Gratings Accessed by Reversible Shape Memory, ACS Appl. Mater. Interfaces 7 (26) (2015) 14288–14293.

[29] T. Xie, J.J. Li, Q. Zhao, Hidden Thermoreversible Actuation Behavior of Nafion and Its Morphological Origin, Macromolecules 47 (3) (2014) 1085–1089.

[30] N. Inverardi, M. Toselli, G. Scalet, M. Messori, F. Auricchio, S. Pandini, Stress-Free Two-Way Shape Memory Effect of Poly(ethylene glycol)/ Poly(ε-caprolactone) Semicrystalline Networks, Macromolecules (2022) 8533–8547.

[31] M.R. Pfau, K.G. McKinzey, A. Roth, M.A. Grunlan, PCL-Based Shape Memory Polymer Semi-IPNs: The Role of Miscibility in Tuning the Degradation Rate, Biomacromolecules 21 (6) (2020) 2493–2501.

[32] D.L. Thomsen, P. Keller, J. Naciri, R. Pink, H. Jeon, D. Shenoy, B.R. Ratna, Liquid crystal elastomers with mechanical properties of a muscle, Macromolecules 34 (17) (2001) 5868–5875.

[33] L. Lu, G. Li, One-way multishape-memory effect and tunable two-way shape memory effect of ionomer poly (ethylene-co-methacrylic acid), ACS Appl. Mater. Interfaces 8 (23) (2016) 14812–14823.

[34] T.Z. Gani, Z.J. Berkson, R. Zhu, J.H. Kang, J.R. Di Iorio, K.W. Chan, D.F. Consoli, S. K. Shaikh, C. Copéret, Y. Román-Leshkov, Promoting active site renewal in heterogeneous olefin metathesis catalysts, Nature 617 (7961) (2023) 524–528.

[35] J.A. de Sousa, J.L. da Silva Sá, J.W. de Mesquita Carneiro, J.M. de Matos, Structural and thermodynamic insights into the coordination preference of norbornadiene with the initiator complex $[RuCl_2(PPh_3)_2(piperidine)]$ in polymerization via olefin metathesis, Phys. Chem. Chem. Phys. 26 (17) (2024) 13164–13171.

[36] W.S. Miao, B. Yang, B.J. Jin, C.J. Ni, H.J. Feng, Y.T. Xue, N. Zheng, Q. Zhao, Y. Q. Shen, T. Xie, An Orthogonal Dynamic Covalent Polymer Network with Distinctive Topology Transformations for Shape- and Molecular Architecture Reconfiguration, Angew. Chem. Int. Edit. 61 (11) (2022) e202109941.

[37] Y.X. Lu, F. Tournilhac, L. Leibler, Z.B. Guan, Making Insoluble Polymer Networks Malleable via Olefin Metathesis, J. Am. Chem. Soc. 134 (20) (2012) 8424–8427.

[38] A.M. Levenson, C.M. Morrison, P.-R. Huang, T.-W. Wang, Z. Carter-Schwendler, M. R. Golder, Ancillary Ligand Lability Improves Control in Cyclic Ruthenium Benzylidene Initiated Ring-Expansion Metathesis Polymerizations, ACS Macro Lett. 12 (10) (2023) 1286–1292.

[39] T. Xiao, Y. Chen, Q. Li, Y. Gao, L. Pan, F. Xuan, All Digital Light Processing-3D Printing of Flexible Sensor, Macromolecules 8 (2) (2023) 2201376.

[40] S.M. Montgomery, F. Demoly, K. Zhou, H. Qi, Pixel-Level Grayscale Manipulation to Improve Accuracy in Digital Light Processing 3D Printing, Adv. Mater. Technol.-US 33 (17) (2023) 2213252.

[41] R. Prabhakaran, P. Pitchipoo, S. Rajakarunakaran, R. Venkatesh, Part E: Journal of Process Mechanical Engineering, Experimental investigation and optimization of process parameters on digital light processing (DLP) 3D printing process based on Taguchi-grey relational analysis, P. I. Mech. Eng. E.-J. Pro. (2024) 09544089241236267.

[42] X.W. Mu, X.J. Li, C. Liao, H. Yu, Y. Jin, B. Yu, L.F. Han, L.K. Chen, Y.C. Kan, L. Song, Y. Hu, Phosphorus-Fixed Stable Interfacial Nonflammable Gel Polymer Electrolyte for Safe Flexible Lithium-Ion Batteries, Adv. Func. Mater. 32 (35) (2022) 2203006.

[43] D.S. Kazybayeva, G.S. Irmukhametova, V.V. Khutoryanskiy, Synthesis of hydrolytically and oxidation-responsive networks using thiol-ene "click" chemistry with pentaerythritol tetrakis(3-mercaptopropionate) and tri/tetra-acrylates, Polym. Advan. Technol. 32 (7) (2021) 2682–2689.

[44] X.W. Mu, X. Zhou, W. Wang, Y.L. Xiao, C. Liao, H. Longfei, Y.C. Kan, L. Song, Design of compressible flame retardant grafted porous organic polymer based separator with high fire safety and good electrochemical properties, Chem. Eng. J. 405 (2021) 126946.

[45] S. Wang, T. Wang, S. Zhang, Z. Dong, V.S. Chevali, Y. Yang, G. Wang, H. Wang, Enhancing fiber-matrix interface in carbon fiber/poly ether ether ketone (CF/PEEK) composites by carbon nanotube reinforcement of crystalline PEEK sizing, Compos. Part. B-Eng. 251 (2023) 110470.

[46] S. Paszkiewicz, P. Lesiak, K. Walkowiak, I. Irska, K. Miądlicki, M. Królikowski, E. Piesowicz, P. Figiel, The Mechanical, Thermal, and Biological Properties of Materials Intended for Dental Implants: A Comparison of Three Types of Poly (aryl-ether-ketones)(PEEK and PEKK), Polymers-Basel 15 (18) (2023) 3706.

[47] I.K. Han, K.I. Song, S.M. Jung, Y. Jo, J. Kwon, T. Chung, S. Yoo, J. Jang, Y.T. Kim, D.S. Hwang, Electroconductive, adhesive, non-swelling, and viscoelastic hydrogels for bioelectronics, Adv. Mater. 35 (4) (2023) 2203431.

[48] A. Paudel, A.N. Crum, Y.J. Wang, A full metal-free flexible ammonium-ion battery with biodegradable hydrogel electrolyte, J. Mater. Chem. A 12 (20) (2024) 11975–11985.

[49] S. Kuchena, A. Paudel, Q. Wu, Y.J. Wang, A novel aqueous zinc-ion battery capable of self-charging at low temperature, J. Mater. Chem. A 12 (5) (2024) 2867–2876.

[50] Z. Wang, Z. Wu, L. Weng, S. Ge, D. Jiang, M. Huang, D.M. Mulvihill, Q. Chen, Z. Guo, A. Jazzar, A roadmap review of thermally conductive polymer composites: critical factors, progress, and prospects, Adv. Func. Mater. 33 (36) (2023) 2301549.

[51] S. Seiffert, Physical chemistry of polymers: A conceptual introduction, Walter De Gruyter GmbH & Co KG (2023).

[52] M. Badreldin, P.S. Ambrosio, E. Garanger, S. Lecommandoux, S. Harrisson, C. Bonduelle, Thermoresponsive polymers: from natural proteins to amino acid based polymer synthesis, Prog. Polym. Sci. (2023) 101752.

[53] S. Koltzenburg, M. Maskos, O. Nuyken, Polymer Chemistry, Springer Nature 2023.

[54] A.P. Murcia, J.M.U. Gomez, J.U. Sommer, L. Ionov, Two-way shape memory polymers: evolution of stress vs evolution of elongation, Macromolecules 54 (12) (2021) 5838–5847.
[55] A. Posada-Murcia, J.M. Uribe-Gomez, S. Förster, J.U. Sommer, M. Dulle, L. Ionov, Mechanism of behavior of two-way shape memory polymer under constant strain conditions, Macromolecules 55 (5) (2022) 1680–1689.
[56] J.Z. Fan, G.Q. Li, High enthalpy storage thermoset network with giant stress and energy output in rubbery state, Nature Communications 9 (2018) 642.
[57] X.L. Li, A. Vazquez-López, J.S.D. Saez, D.Y. Wang, Recent advances on early-stage fire-warning systems: mechanism, performance, and perspective, Nano-Micro Lett. 14 (1) (2022) 197.
[58] W.F. Chen, B.W. Liu, S.M. Pei, X.M. Jiang, G.C. Guo, [K2PbX][Ga7S12](X= Cl, Br, I): the first lead-containing cationic moieties with ultrahigh second-harmonic generation and band gaps exceeding the criterion of 2.33 eV, Adv. Sci. 10 (13) (2023) 2207630.
[59] C.B. Hao, K.B. Wang, Z. Wang, R.X. Duan, H. Liu, M.M. Huang, W.T. Liu, S.Q. He, C.S. Zhu, Triple one-way and two-way shape memory poly(ethylene-co-vinyl acetate)/poly(ε-caprolactone) immiscible blends, J. Appl. Polym. Sci. 139 (1) (2022) 51426.
[60] H.F. Lu, M. Wang, X.M. Chen, B.P. Lin, H. Yang, Interpenetrating Liquid-Crystal Polyurethane/Polyacrylate Elastomer with Ultrastrong Mechanical Property, J. Am. Chem. Soc. 141 (36) (2019) 14364–14369.
[61] H.H. Qin, P.T. Mather, Combined One-Way and Two-Way Shape Memory in a Glass-Forming Nematic Network, Macromolecules 42 (1) (2009) 273–280.
[62] J.M. Raquez, S. Vanderstappen, F. Meyer, P. Verge, M. Alexandre, J.M. Thomassin, C. Jérôme, P. Dubois, Design of Cross-Linked Semicrystalline Poly(ε-caprolactone)-Based Networks with One-Way and Two-Way Shape-Memory Properties through Diels-Alder Reactions, Chem.-Eur. J. 17 (36) (2011) 10135–10143.
[63] S.J. Hong, W.R. Yu, J.H. Youk, Two-way shape memory behavior of shape memory polyurethanes with a bias load, Smart Mater. Struct. 19 (3) (2010) 035022.
[64] T. Chung, A. Rorno-Uribe, P.T. Mather, Two-way reversible shape memory in a semicrystalline network, Macromolecules 41 (1) (2008) 184–192.
[65] L. Ma, J. Zhao, X.Y. Wang, M. Chen, Y.R. Liang, Z.W. Wang, Z.N. Yu, R.C. Hedden, Effects of carbon black nanoparticles on two-way reversible shape memory in crosslinked polyethylene, Polymer 56 (2015) 490–497.
[66] J. Zotzmann, M. Behl, D. Hofmann, A. Lendlein, Reversible Triple-Shape Effect of Polymer Networks Containing Polypentadecalactone- and Poly(ε-caprolactone)-Segments, Adv. Mater. 22 (31) (2010) 3424–3429.
[67] M.M. Huang, X. Dong, L.L. Wang, J. Zhao, G.M. Liu, D.J. Wang, Two-way shape memory property and its structural origin of cross-linked poly(ε-caprolactone), RSC Adv. 4 (98) (2014) 55483–55494.
[68] B. Wang, X. Lai, H. Li, C. Jiang, J. Gao, X. Zeng, Interfaces, Multifunctional MXene/chitosan-coated cotton fabric for intelligent fire protection, Interfaces 13 (19) (2021) 23020–23029.
[69] M. Zhang, M. Wang, M. Zhang, C. Yang, Y. Li, Y. Zhang, J. Hu, G. Wu, interfaces, Flexible and thermally induced switchable fire alarm fabric based on layer-by-layer self-assembled silver sheet/Fe3O4 nanowire composite, Interfaces 11 (50) (2019) 47456–47467.
[70] C. Jiang, J. Chen, X. Lai, H. Li, X. Zeng, Y. Zhao, Q. Zeng, J. Gao, Z. Wu, Y. Qiu, Mechanically robust and multifunctional polyimide/MXene composite aerogel for smart fire protection, Chem. Eng. J. 434 (2022) 134630.
[71] B. Yuan, Y. Wang, G. Chen, F. Yang, H. Zhang, C. Cao, B. Zuo, Nacre-like graphene oxide paper bonded with boric acid for fire early-warning sensor, J. Hazard. Mater. 403 (2021) 123645.
[72] B. Chen, Y. Liu, K. Wu, M. Lu, E. Jiao, J. Shi, M. Lu, Calorimetry, Enhanced thermal conductivity and fire safety of flexible hybrid film via synergistic effects between boron nitride and functionalized graphene, J. Therm. Anal. Calorim. 147 (6) (2022) 4047–4058.
[73] Z.-R. Yu, M. Mao, S.-N. Li, Q.-Q. Xia, C.-F. Cao, L. Zhao, G.-D. Zhang, Z.-J. Zheng, J.-F. Gao, L.-C. Tang, Facile and green synthesis of mechanically flexible and flame-retardant clay/graphene oxide nanoribbon interconnected networks for fire safety and prevention, Chem. Eng. J. 405 (2021) 126620.
[74] C.R. Cao, B.H. Yuan, Thermally induced fire early warning aerogel with efficient thermal isolation and flame-retardant properties, Polym. Advan. Technol. 32 (5) (2021) 2159–2168.
[75] B.F. Nan, K. Wu, Z.C. Qu, L.Q. Xiao, C.G. Xu, J. Shi, M.G. Lu, A multifunctional thermal management paper based on functionalized graphene oxide nanosheets decorated with nanodiamond, Carbon 161 (2020) 132–145.
[76] G.Q. Chen, B.H. Yuan, Y. Wang, X.F. Chen, C.Y. Huang, S. Shang, H.J. Tao, J. Liu, W.K. Sun, P. Yang, G.B. Shi, Nacre-biomimetic graphene oxide paper intercalated by phytic acid and its ultrafast fire-alarm application, J. Colloid. Interf. Sci. 578 (2020) 412–421.
[77] Q. Wu, L.X. Gong, Y. Li, C.F. Cao, L.C. Tang, L.B. Wu, L. Zhao, G.D. Zhang, S.N. Li, J.F. Gao, Y.J. Li, Y.W. Mai, Efficient Flame Detection and Early Warning Sensors on Combustible Materials Using Hierarchical Graphene Oxide/Silicone Coatings, ACS Nano 12 (1) (2018) 416–424.
[78] C.F. Cao, B. Yu, Z.Y. Chen, Y.X. Qu, Y.T. Li, Y.Q. Shi, Z.W. Ma, F.N. Sun, Q.H. Pan, L.C. Tang, P.A. Song, H. Wang, Fire Intumescent, High-Temperature Resistant, Mechanically Flexible Graphene Oxide Network for Exceptional Fire Shielding and Ultra-Fast Fire Warning, Nano-Micro Lett. 14 (1) (2022) 92.